COMMUNICATIONS BIOLOGY

ARTICLE

DOI: 10.1038/s42003-018-0162-z OPEN

Doxorubicin induces caspase-mediated proteolysis of KV7.1

Anne Strigli[1], Christian Raab[1], Sabine Hessler[2], Tobias Huth[2], Adam J.T. Schuldt[3], Christian Alzheimer[2], Thomas Friedrich[4], Paul W. Burridge[3], Mark Luedde[5] & Michael Schwake[1,6,7]

K_v7.1 (KCNQ1) coassembles with KCNE1 to generate the cardiac I_{Ks}-channel. Gain- and loss-of-function mutations in *KCNQ1* are associated with cardiac arrhythmias, highlighting the importance of modulating I_{Ks} activity for cardiac function. Here, we report proteolysis of K_v7.1 as an irreversible posttranslational modification. The identification of two C-terminal fragments of K_v7.1 led us to identify an aspartate critical for the generation of one of the fragments and caspases as responsible for mediating proteolysis. Activating caspases reduces K_v7.1/KCNE1 currents, which is abrogated in cells expressing caspase-resistant channels. Enhanced cleavage of K_v7.1 can be detected for the LQT mutation G460S, which is located adjacent to the cleavage site, whereas a calmodulin-binding-deficient mutation impairs cleavage. Application of apoptotic stimuli or doxorubicin-induced cardiotoxicity provokes caspase-mediated cleavage of endogenous I_{Ks} in human cardiomyocytes. In summary, caspases are novel regulatory components of I_{Ks} channels that may have important implications for the molecular mechanism of doxorubicin-induced cardiotoxicity.

[1] Institute of Biochemistry, Christian Albrechts University of Kiel, Otto-Hahn-Platz 9, 24118 Kiel, Germany. [2] Institute of Physiology and Pathophysiology, Friedrich-Alexander-Universität Erlangen-Nürnberg, Universitätsstr. 17, 91054 Erlangen, Germany. [3] Department of Pharmacology and Center for Pharmacogenomics, Feinberg School of Medicine, Northwestern University, 320 East Superior Street, Searle Building 8-450, Chicago, IL 60611, USA. [4] Institut für Chemie PC 14, Technische Universität Berlin, Straße des 17. Juni 135, 10623 Berlin, Germany. [5] Department of Internal Medicine III, University Hospital Schleswig-Holstein, Campus Kiel, Arnold-Heller-Str. 3, 24105 Kiel, Germany. [6] Faculty of Chemistry/Biochemistry III, University of Bielefeld, Universitätsstr. 25, 33615 Bielefeld, Germany. [7] Present address: Department of Neurology, Northwestern University Feinberg School of Medicine, 303 East Chicago Avenue, Chicago, IL 60611-4296, USA. These authors contributed equally: Anne Strigli, Christian Raab. Correspondence and requests for materials should be addressed to M.S. (email: schwake@northwestern.edu)

Voltage-gated potassium channels (K_v) form a protein class comprising 40 members in humans, which can be grouped into 12 families[1]. Among these, the K_v7 (KCNQ) family has attracted special attention since mutations in the five *KCNQ* genes cause heritable diseases, highlighting their physiological importance[2,3]. Dominant-negative mutations in the gene encoding $K_v7.1$ are associated with cardiac arrhythmias contributing to LQT syndrome[4], whereas patients carrying loss-of-function mutations on both alleles additionally suffer from severe congenital hearing loss[5]. Gain-of-function mutations were found in patients with a form of autosomal dominant atrial fibrillation[6], highlighting the important functions of $K_v7.1$ in the heart and inner ear. In both tissues, the α-subunit $K_v7.1$ coassembles with the β-subunit KCNE1, composing an ion channel conducting the slow component of the delayed rectifier potassium current, I_{Ks}, which is indispensable for shaping the cardiac action potential[7,8]. Another important physiological function of $K_v7.1$ was discovered by genome-wide association studies, in which single nucleotide polymorphisms in the *KCNQ1* locus were associated with type 2 diabetes in several populations[9,10]. In nonexcitable (e.g., polarized thyroid, intestinal and tracheal epithelial) cells, $K_v7.1$ associates with the β-subunits KCNE2 and KCNE3, respectively. The latter β-subunits, in contrast to KCNE1, reduce the voltage-dependent gating of the outwardly rectifying $K_v7.1$ α-subunit, resulting in constitutively open channels. The $K_v7.1$/KCNE2 channel complex has been described to be crucial for thyroid hormone biosynthesis[11], whereas $K_v7.1$/KCNE3 heterodimers play an important role in chloride secretion across tracheal and intestinal epithelia[12]. In the intestine, transposon-based forward mutagenesis genetic screens identified *KCNQ1* as a cancer susceptibility gene[13] and low expression of $K_v7.1$ was found in patients with colorectal cancer[14]. However, the role of $K_v7.1$ in cancer development has yet to be established.

Channels formed from K_v7 α-subunits share some structural features with *Shaker*-related K_v channels, such as a common core structure of six transmembrane domains (S1−S6) including a voltage-sensing domain (S1−S4) and a pore domain (S5−S6)[2]. One striking difference, however, is the presence of a large cytoplasmic C-terminal domain in K_v7 channels, which is important for gating, assembly, and intracellular trafficking of the channel and comprises four helical domains (A−D) (reviewed in Haitin and Attali[15]). Whereas helices A and B mediate calmodulin binding[16], helices C and D form the subunit interaction domain[17], which consists of a bipartite coiled-coil motif that is crucial for subunit-specific interaction and tetramerization of the K_v7 α-subunits[18,19]. For $K_v7.1$, it has also been shown that the A-kinase anchoring protein yotiao binds to helix D, leading to the recruitment of protein kinase A (PKA) and protein phosphatase 1, thereby forming a macromolecular complex important for regulating I_{Ks} activity[20]. In addition to PKA-mediated phosphorylation, ubiquitination and sumoylation have been reported to be important for regulation of $K_v7.1$ activity at the post-translational level[21,22].

Anthracyclines such as doxorubicin are well-established and effective antineoplastic agents, commonly used for the treatment of cancers. However, doxorubicin treatment has cardiotoxicity as a severe side effect, which can lead to QT prolongation and heart failure[23,24]. Increased production of reactive oxygen species (ROS) and the induction of mitochondrial dysfunction are well-described molecular mechanisms of doxorubicin-induced cardiomyopathy, resulting in an activation of apoptotic pathways, finally leading to caspase activation[25]. Dexrazoxane, a cardioprotective agent, acts in the same pathway by chelating Fe^{2+} ions more effectively than doxorubicin. While Fe^{2+} ions bound to doxorubicin are efficiently oxidized to Fe^{3+}, resulting in release of electrons, which are rapidly transferred to produce ROS, the redox activity of dexrazoxane on Fe^{2+} ions is much lower, so that the Fe^{2+}-scavenging activity and the consequently reduced ROS production by dexrazoxane have been suggested to underlie the alleviating effect on cardiotoxicity[26].

Caspases are cysteine proteases, which specifically cleave their substrates at the C-terminal side of an aspartic acid and play important roles in numerous aspects of physiology such as apoptosis, aging, development, and inflammation[27]. Caspases are well known for their executive role in apoptosis and can be grouped into initiator (caspase 2, 8–10) and effector caspases (caspase 3, 6 and 7)[28]. Activation of caspases is triggered either by the extrinsic pathway, mediated by ligand binding to death receptors and activation of the initiator caspase 8, or by the intrinsic pathway[28]. In the latter case, mitochondrial membranes are permeabilized by the proapoptotic proteins BCL-2 and BAX, leading to a loss of mitochondrial transmembrane potentials and to the release of other proapoptotic proteins such as cytochrome C into the cytosol, which results in the activation of the initiator caspase 9. Activated caspases 8 and 9 specifically cleave effector caspases, which finally execute apoptosis[28]. With the exception of caspase 14, all other caspases in humans have been implicated in inflammation[28]. Moreover, altered caspase expression levels have been correlated with ageing[29] and heart failure[30,31]. Recently, it has become evident that caspases also have nonapoptotic and noninflammatory functions, such as regulation of long-term depression[32] or organelle removal during terminal differentiation[33].

By using $K_v7.1$-specific antibodies directed against an epitope on the channel's C-terminus, we detected two c-terminal fragments, leading us to the hypothesis that $K_v7.1$ is processed by unknown proteases. In the present study, we identify $K_v7.1$ as a novel substrate for caspases, which may have important implications for understanding the role of $K_v7.1$ in cardiac arrhythmias and its function as a tumor suppressor. Our data suggest that caspase-mediated proteolysis of $K_v7.1$ leads to decreased $K_v7.1$-mediated currents, representing a novel regulatory mechanism for modulating $K_v7.1$ channel activity. Furthermore, we show that $K_v7.1$ cleavage is induced upon administration of doxorubicin, which efficiently activates caspase 3 in human cardiomyocytes. To our knowledge, $K_v7.1$ is the first example of a voltage-gated potassium channel that acts as a substrate for caspases.

Results

Proteolysis of $K_v7.1$ produces C-terminal fragments. We and others[34,35] have noted the occurrence of $K_v7.1$ C-terminal fragments in transfected cells, when antibodies directed against epitopes on the $K_v7.1$ C-terminus were used, which prompted us to further analyze the specificity of these fragments. We found C-terminal fragments of the full-length $K_v7.1$ channel in lysates derived from transiently transfected cells with human or murine $K_v7.1$ cDNA constructs (Fig. 1a). Two fragments with a molecular mass of about ~40 and ~28 kDa can be detected in addition to the full-length form of $K_v7.1$ at ~70 kDa, when an antibody directed against a C-terminally derived peptide of $K_v7.1$ was used (Fig. 1a and Supplementary Fig. 1A). Next, we demonstrated the specificity of the $K_v7.1$ antibody by the absence of signals in various tissues derived from $K_v7.1$-deficient mice, which do not show detectable $K_v7.1$ in immunoblots (Supplementary Fig. 1B). As expected, we found the highest expression of Kv7.1 in murine heart, when compared to kidney and pancreas, further supporting the specificity of the antibody (Supplementary Fig. 1B). C-terminal fragments of $K_v7.1$ were also detectable in cells transfected with a cDNA construct of human $K_v7.1$ tagged at the C-terminus with an MYC epitope (Fig. 1b). Immunoblots with either the MYC or the $K_v7.1$ antibodies resulted in the same

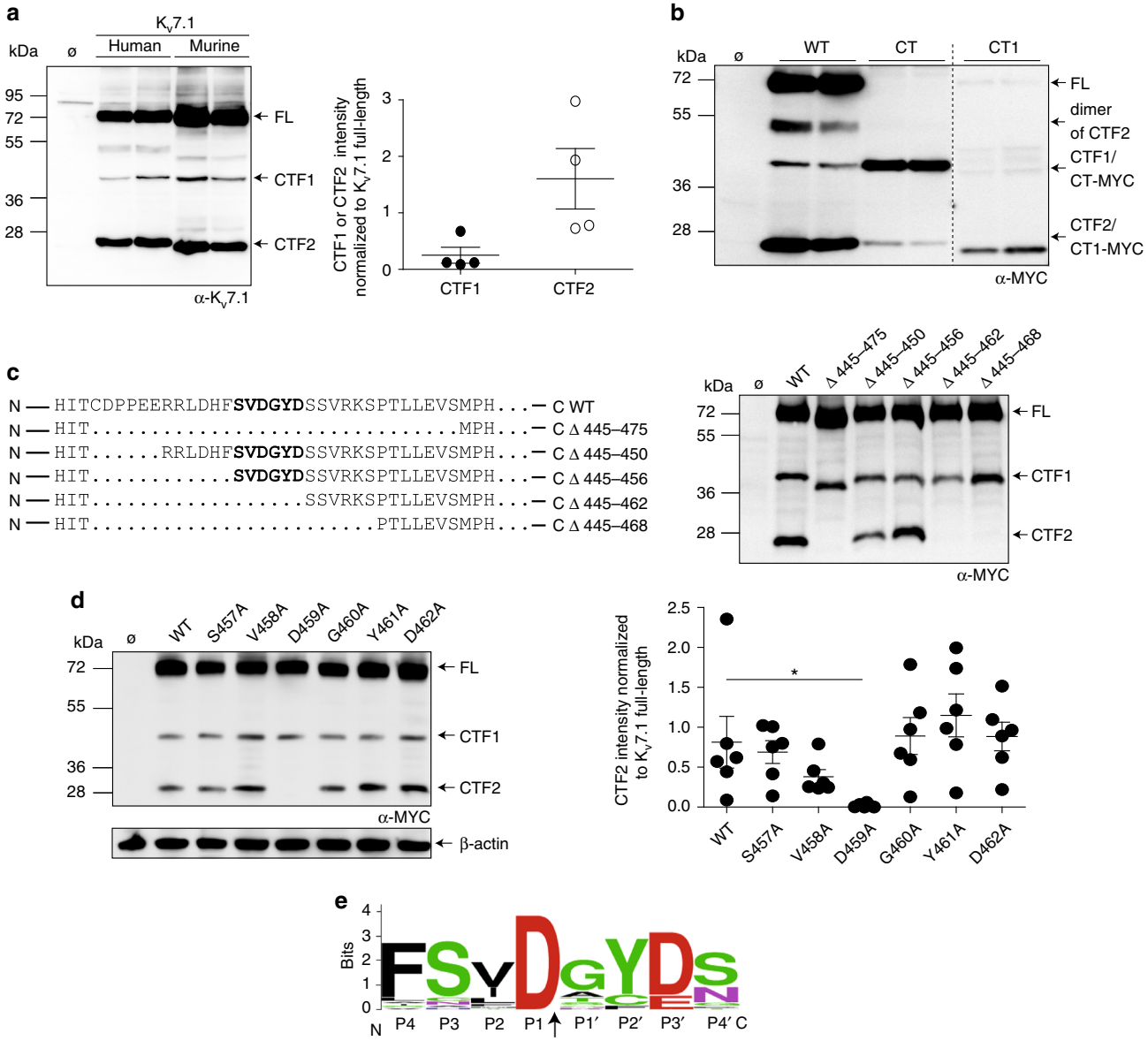

Fig. 1 Kv7.1 is cleaved at aspartate 459. **a** Western blot analysis of HeLa cell lysates overexpressing human and murine $K_v7.1$ constructs. Untransfected cells (Ø) served as negative control. Densitometric analysis of four independent experiments of the CTF1 or CTF2 band intensity normalized to the full-length $K_v7.1$ band intensity. **b** Immunoblot analysis of lysates derived from HeLa cells overexpressing indicated constructs. Untransfected cells (Ø) served as negative control. **c** Schematic illustration of different deletion constructs in the linker region between helices A and B. HeLa cell lysates overexpressing indicated constructs analyzed by western blot. Untransfected cells (Ø) served as negative control. **d** Alanine scan of position 457 to 462. Lysates from HeLa cells overexpressing indicated constructs were used for western blot analysis. Untransfected cells (Ø) served as negative control. Densitometric analysis of six independent experiments of CTF2 band intensity normalized to $K_v7.1$ full-length band intensity. Statistics were tested with one-way-ANOVA followed by Bonferroni's Multiple Comparison test. **e** Cleavage site sequence logo of $K_v7.1$ derived from 32 different species. Logo was created with weblogo.berkley.edu and adapted accordingly. The arrow indicates the cleavage site. **a** Anti-$K_v7.1$ antibody. **b**–**d** Anti-MYC antibody. All dot blots are shown as mean and error bars as SEM

pattern. Next, we analyzed neonatal rat ventricular cardiomyocytes (NRVMs) for endogenous expression of $K_v7.1$. Again, we found immunoreactive bands resembling full-length $K_v7.1$ (~70 kDa) and bands at ~40 and ~28 kDa, albeit with low intensity (Supplementary Fig. 1C). We concluded that $K_v7.1$ is cleaved twice at its C-terminus, resulting in three fragments: The N-terminal fragment comprising the cytoplasmic N-terminus and the membrane-embedded part of the protein and two C-terminal fragments showing immunoreactivity with the $K_v7.1$ antibody, which we termed CTF1 (~40 kDa) and CTF2 (~28 kDa) (Supplementary Fig. 1A).

To determine the cleavage sites, we generated two $K_v7.1$ constructs: one comprising the complete C-terminus (CT, starting with glycine at position 348), and the other beginning at helix B (CT1 beginning with amino acid 505) (Supplementary Fig. 1A). After expression of these fragments in HeLa cells, we compared the size of the resulting bands of CT and CT1 with the C-terminal fragments CTF1 and CTF2 (Fig. 1c). CT and CTF1 migrate at the same molecular weight, whereas CTF2 runs slightly slower than the CT1 construct. From these data, we conclude that the cleavage site for the generation of CTF1 resides between the end of the transmembrane domain S6 and helix A, while the

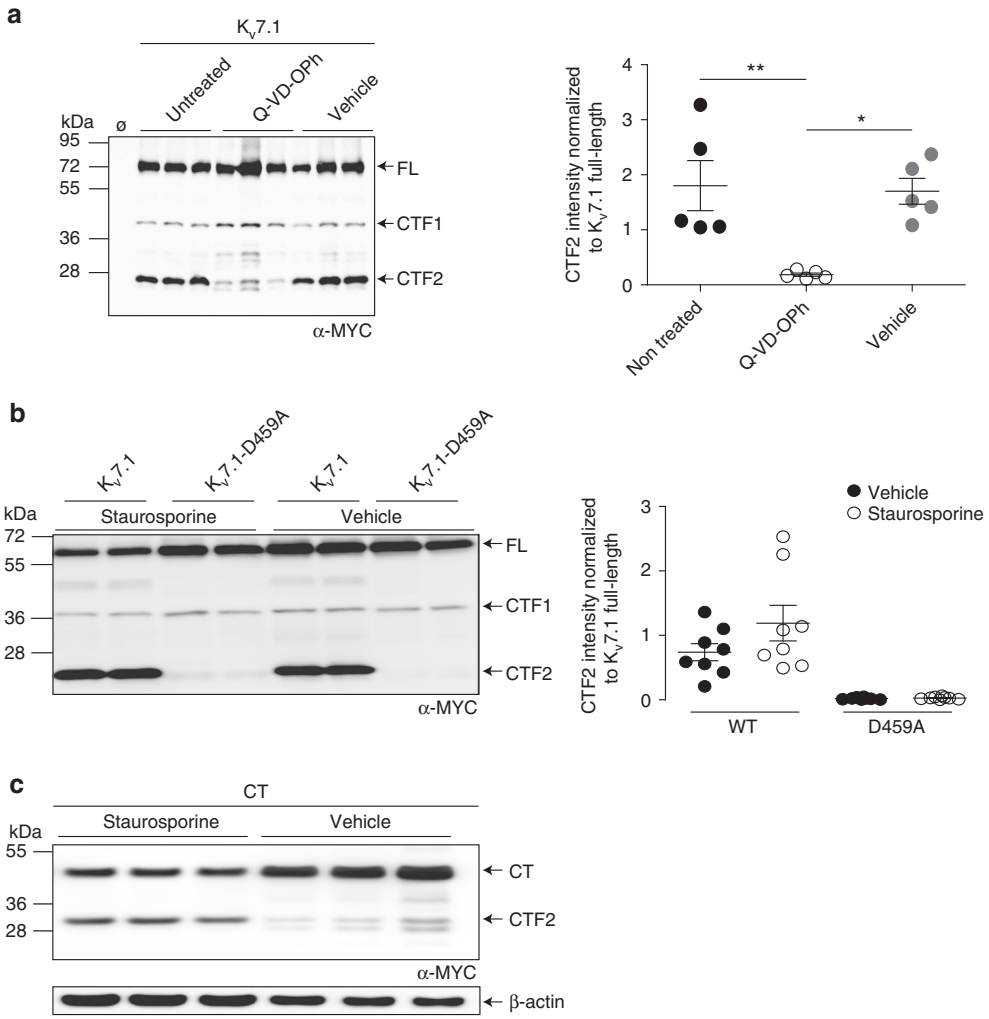

Fig. 2 Cleavage of Kv7.1 occurs during apoptosis. **a** Western blot analysis of Cos7 cells overexpressing K_v7.1-MYC treated for 12 h with 450 nmol per L Q-VD-OPh. Untransfected (Ø), nontreated and vehicle-treated cells served as negative controls. Densitometric analysis of five independent experiments of CTF2 band intensity normalized to K_v7.1 full-length band intensity. Statistics were tested with one-way-ANOVA followed by Bonferroni's Multiple Comparison test. **b** Lysates derived from HeLa cells expressing K_v7.1-MYC and K_v7.1-D459A-MYC constructs treated with 1 µmol per L staurosporine for 8 h analyzed by immunoblotting. Untransfected (Ø) and vehicle-treated cells served as negative controls. Densitometric analysis of eight independent experiments of the CTF2 band intensity normalized to K_v7.1 full-length band intensity. **c** Western blot analysis of HeLa cell lysates overexpressing CT-MYC construct treated for 8 h with 1 µmol per L staurosporine. Vehicle-treated cells served as negative controls. **a**–**c** Anti-MYC antibody, **a**, **c** anti-β-actin antibody. All dot blots are shown as mean and error bars as SEM

cleavage site for CTF2 likely lies within the loop region between helices A and B in the C-terminus of K_v7.1.

Since CTF2 is the most abundant C-terminal fragment (Fig. 1a, b, Supplementary Fig. 1C), we focused our analysis on the region between helices A and B. We generated five K_v7.1 constructs with varying deletions within this linker region (Fig. 1c). Immunoblot analysis of lysates derived from cells expressing these constructs revealed that a stretch of six amino acids ($S^{457}VDGYD^{462}$) was essential for the occurrence of CTF2 (Fig. 1c). Next, we performed an alanine scan over the SVDGYD region to define the precise cleavage site. Mutating the aspartate at position 459 to an alanine resulted in a complete loss of CTF2 generation, whereas mutating the other five residues (including Asp-462) appeared to have no significant effect (Fig. 1d). These data demonstrate that K_v7.1 is cleaved within the SVDGYD motif at position D459 by a protease, which requires an aspartate. However, K_v7.1 is the only member within the Kv7 family carrying an aspartate at this position (Supplementary Fig. 1D). This aspartate is highly conserved within K_v7.1 protein sequences derived from over 20 different species (Fig. 1e and Supplementary Fig. 2).

K_v7.1 is cleaved by caspases upon apoptosis. To identify the protease responsible for the generation of CTF2, we searched the Merops Database for proteases that require an aspartate in the cleavage site[36]. Since caspases critically depend on an aspartate at the P1 position[27], we used two caspase inhibitors (Q-VD-OPH and Z-VAD(OMe)-FMK) to determine whether caspases are responsible for the generation of CTF2. Both compounds effectively inhibited the generation of CTF2 but not CTF1 (Fig. 2a and Supplementary Fig. 3). To activate caspases, we induced apoptosis in cells overexpressing wild-type K_v7.1 and the D459A mutant by applying staurosporine, a nonselective protein kinase inhibitor widely used as a proapoptotic stimulus. Whereas wild-type K_v7.1 was efficiently proteolysed, the D459A mutant appeared resistant to staurosporine treatment (Fig. 2b), demonstrating that the D459A mutant is insensitive to staurosporine-induced caspase

activation and cleavage. Next, we asked whether the generation of the CTF2 was dependent on the full-length K_v7.1 α-subunit. We therefore expressed the CT construct (Supplementary Fig. 1A) under control and apoptotic conditions. Again, an increase in CTF2 generation could be observed upon staurosporine treatment (Fig. 2c) indicating that cleavage can occur independent from the membrane-embedded part of the Kv7.1 protein. To gain deeper insight into the involvement of caspases in K_v7.1 proteolysis, we applied staurosporine and the specific caspase 8 inhibitor II to cells expressing K_v7.1. As shown in Fig. 3a, inhibition of caspase 8 efficiently blocked activation of downstream caspase 3 and the generation of CTF2 dose-dependently, demonstrating that the staurosporine-induced CTF2 generation is mediated by caspases.

To address the question whether caspase 3, one of the major effector caspases, is solely responsible for K_v7.1 cleavage at position D459, we used a human breast carcinoma MCF-7 cell line, which is deficient for caspase 3 [37]. Overexpression of K_v7.1 in MCF-7 cells still resulted in the generation of CTF2 albeit to a lower extent (Fig. 3b, eGFP labeled lane). Whereas cotransfection of K_v7.1 together with wild-type caspase-3 restored CTF2 production, the overexpression of an inactive form of caspase-3 led to a reduction of CTF2 levels (Fig. 3b) likely by protecting K_v7.1 from endogenous caspases. To determine whether all caspases cleave K_v7.1 to the same extent, we coexpressed K_v7.1 with at least one caspase of each group, namely caspases 1, 2, 3, 7, and 8. Immunoblots revealed that all tested caspases are able to generate CTF2 (Fig. 3c). Stronger cleavage could be observed by overexpression of the initiator caspase 1, 2 and 8, which might be due to an activation of downstream effector caspases. Nevertheless, these data suggest that K_v7.1 is a substrate of all analyzed caspases.

To demonstrate that endogenous K_v7.1, embedded in the I_{Ks} channel complex undergoes caspase-mediated proteolysis, we treated murine cardiac muscle cells (HL-1 cells[38]) with increasing concentrations of staurosporine, confirming a dose-dependent occurrence of CTF2 (Fig. 3d). Notably, full-length K_v7.1 channel was efficiently cleaved at higher staurosporine concentrations. In summary, our data strongly suggest that K_v7.1 is cleaved by caspases at an aspartate at position 459.

Functional impact of proteolysis on K_v7.1/KCNE1 channels. To analyze the functional impact of caspase-mediated cleavage of K_v7.1 upon induction of apoptosis, we cotransfected HEK 293T cells with wild-type Kv7.1 and the D459A mutant together with KCNE1 and measured whole-cell currents under staurosporine treatment and control conditions (Fig. 4a). Drug treatment produced a small but significant reduction of K_v7.1/KCNE1 currents, whereas currents generated by K_v7.1 D459A/KCNE1 channels remained unaffected (Fig. 4b). Cells were harvested after patch-clamp measurements and were subjected to immunoblot analysis to probe for CTF2. Again, we were able to detect CTF2 in cells expressing wild-type K_v7.1 but not the D459A mutant (Supplementary Fig. 3B). One possible explanation for the small functional effect of caspase-mediated cleavage on Kv7.1/KCNE1-mediated currents could be a protective effect of KCNE1 on K_v7.1. Since the majority of our analysis so far was done using cells expressing homomeric Kv7.1 channels, we therefore compared the generation of CTF2 in presence and absence of KCNE1. As shown in Fig. 4c, Kv7.1 is efficiently cleaved upon caspase activation even in the presence of KCNE1 indicating that the β-subunit is not shielding the heteromeric Kv7.1/KCNE1 complex from proteolysis. Subsequently, we performed surface biotinylation experiments to prove that the Kv7.1/KCNE1 heteromeric channels can be processed at the plasma membrane by caspases as demonstrated by the presence of CTF2 in the isolated fraction of cell surface proteins (Fig. 4d). Furthermore, these data suggest that CTF2 is, under this condition, still associated with the apoprotein complex. In summary, these data strongly suggest that the activity of heteromeric K_v7.1/KCNE1 channels can be modified by caspase-mediated cleavage in the C-terminus of Kv7.1.

Identifying long-QT mutations modulating K_v7.1 proteolysis. Next, we tested if disease-causing mutations in K_v7.1 can interfere with the generation of CTF2 and focused on the LQT1 mutation G460S, which is located just one amino acid downstream of the aspartate residue important for Kv7.1 proteolysis (Fig. 4d). Immunoblot analysis of the G460S mutant protein demonstrated significantly increased CTF2 levels when compared to wild-type K_v7.1, indicating that this LQT1 mutation renders Kv7.1 more susceptible to caspase-mediated cleavage even under non-staurosporine treatment conditions (Fig. 4d). This observation is in line with the finding that this mutation causes a decrease in I_{Ks}-like currents[39].

The caspase cleavage site resides in an approximately 80 amino acid-long intervening loop between helices A and B (Fig. 4d). Both helices contain an IQ motif, which is important for calmodulin binding (Fig. 4d). Recently, it has been suggested by crystallography, molecular modeling, biochemical, and functional analyses that one bifunctional calmodulin molecule embraces both helices from one K_v7.1 subunit[34]. Given the important role of calmodulin for K_v7.1 function, we asked whether LQT1-associated mutations within the calmodulin binding sites interfere with CTF2 generation. Indeed, the analyses of the K_v7.1 A372D mutation, which is located close to the calmodulin binding motif in helix A, revealed no detectable CTF2 in immunoblots (Fig. 4d). Coimmunoprecipitations proved that the A372D mutation impaired the interaction of endogenous calmodulin with K_v7.1 (Fig. 4e), suggesting that calmodulin binding is necessary for caspase-mediated proteolysis of K_v7.1.

Doxorubicin induces K_v7.1 proteolysis in cardiomyocytes. It is well known that cancer treatment by the common antineoplastic doxorubicin is hindered by severe cardiotoxic side effects, and there is strong evidence in the literature that doxorubicin leads to caspase activation in cardiomyocytes[40]. In order to determine whether interference with cardiac function by doxorubicin also involves caspase-mediated cleavage of Kv7.1, we treated human-induced pluripotent stem cell-derived cardiomyocytes with staurosporine and doxorubicin. In total lysates derived from untreated human-induced pluripotent stem cell-derived cardiomyocytes, we could only detect trace amounts of CTF2, when we used the C-terminal K_v7.1 antibody to precipitate K_v7.1 (compare Fig. 5a and Supplementary Fig. 3C). We were also unable to detect CTF2 in murine cardiomyocytes (Fig. 3d) and tissue (Supplementary Fig. 1B), suggesting that baseline levels of CTF2 and likely K_v7.1 proteolysis are rather low. However, staurosporine and doxorubicin activated caspase 3 as indicated by the occurrence of cleaved-active forms and a reduction of the inactive zymogen of the protease (Fig. 5a). Doxorubicin treatment at higher concentration appeared to be more efficient in producing active caspase 3, which correlated with a higher abundance of CTF2 and a strong reduction of monomeric and tetrameric forms of Kv7.1 (Fig. 5a). Interestingly, we detected a potentially dimeric form of Kv7.1 at 150 kDa in staurosporine- and doxorubicin-treated cells, suggesting that the caspase-mediated destruction of tetramers results in Kv.7.1 dimers in human-induced pluripotent stem cell-derived cardiomyocytes (Fig. 5a). Nevertheless, lower doses of doxorubicin failed to produce similar levels of CTF2, which correlated with a decrease in caspase 3 activation (Fig. 5b).

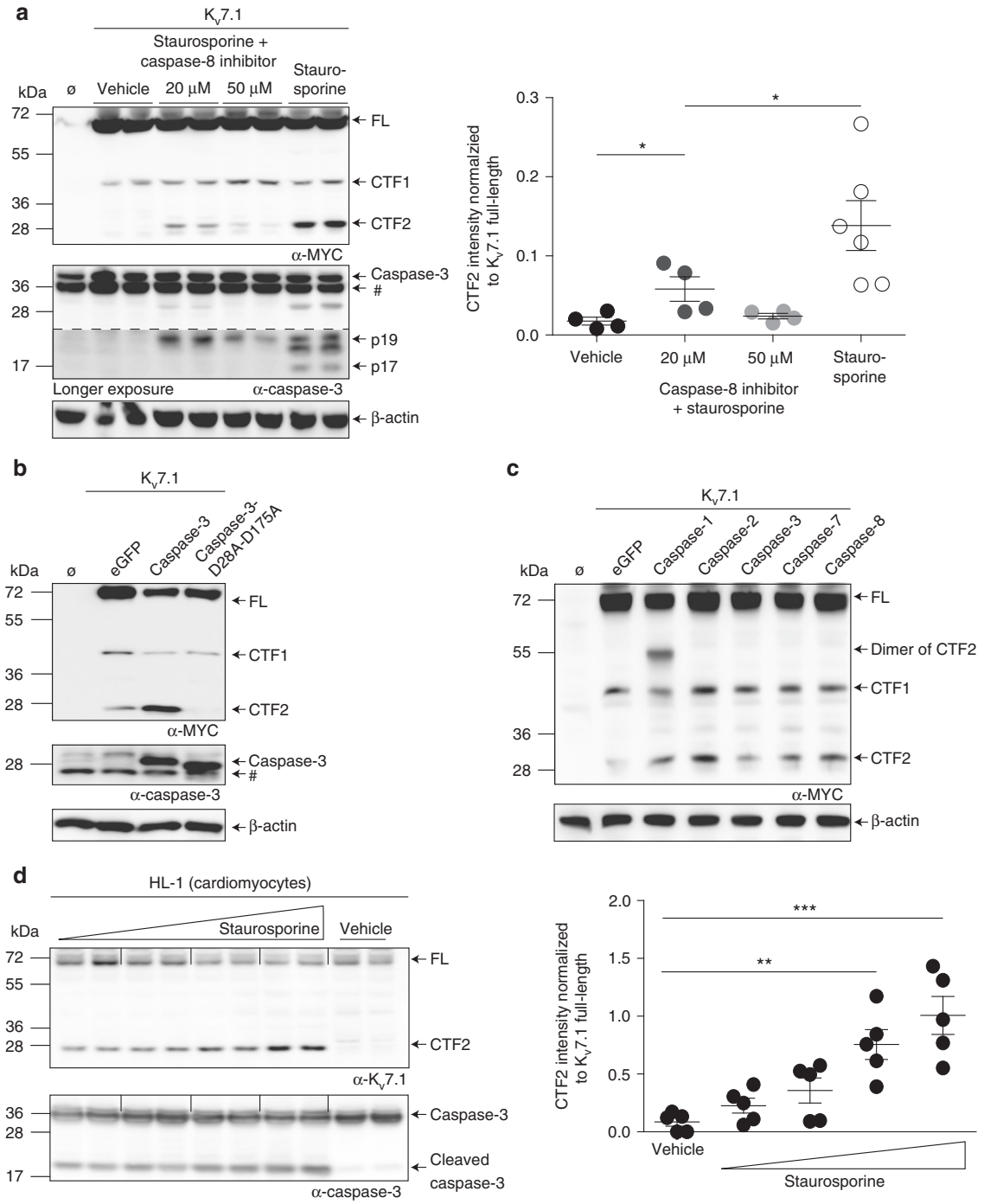

Fig. 3 Caspases are responsible for the generation of CTF2. **a** Western blot analysis of lysates derived from HEK 293T cells stably expressing K_v7.1-MYC treated with either 1 μmol per L staurosporine for 6 h or treated with 1 μmol per L staurosporine for 6 h and pretreated for 2 h with 20 or 50 μmol per L of a caspase-8 inhibitor II. Untransfected (Ø) and vehicle-treated cells served as negative controls. Densitometric analysis of 4–6 independent experiments of the CTF2 band intensity normalized to K_v7.1 full-length band intensity. Statistics were tested with one-way-ANOVA followed by Bonferroni's Multiple Comparison test. # indicates nonspecific binding of the antibody. **b** MCF-7 lysates expressing K_v7.1-MYC and caspase-3 or caspase-3-D28A-D175A analyzed by immunoblot. Untransfected (Ø) and eGFP-transfected cells served as negative controls. # indicates nonspecific binding of the antibody. **c** Lysates of HEK 293T cells stably expressing K_v7.1 and coexpressing indicated caspases analyzed by immunoblot. Untransfected (Ø) and eGFP-transfected cells served as negative controls. **d** Lysates of HL-1 cells treated for 6.5 h with 0.5, 1, 1.5 and 2 μmol per L of staurosporine analyzed by immunoblot. Vehicle-treated cell lysates served as negative control. Densitometric analysis of CTF2 band intensity normalized to Kv7.1 full-length band intensity of five independent experiments. Statistics were tested with one-way-ANOVA followed by Bonferroni's Multiple Comparison test. **a**–**c** Anti-MYC antibody. Anti-β-actin antibody. **a**, **b**, **d** Anti-caspase-3 antibody. **d** Anti-K_v7.1 antibody. All dot blots are shown as mean and error bars as SEM

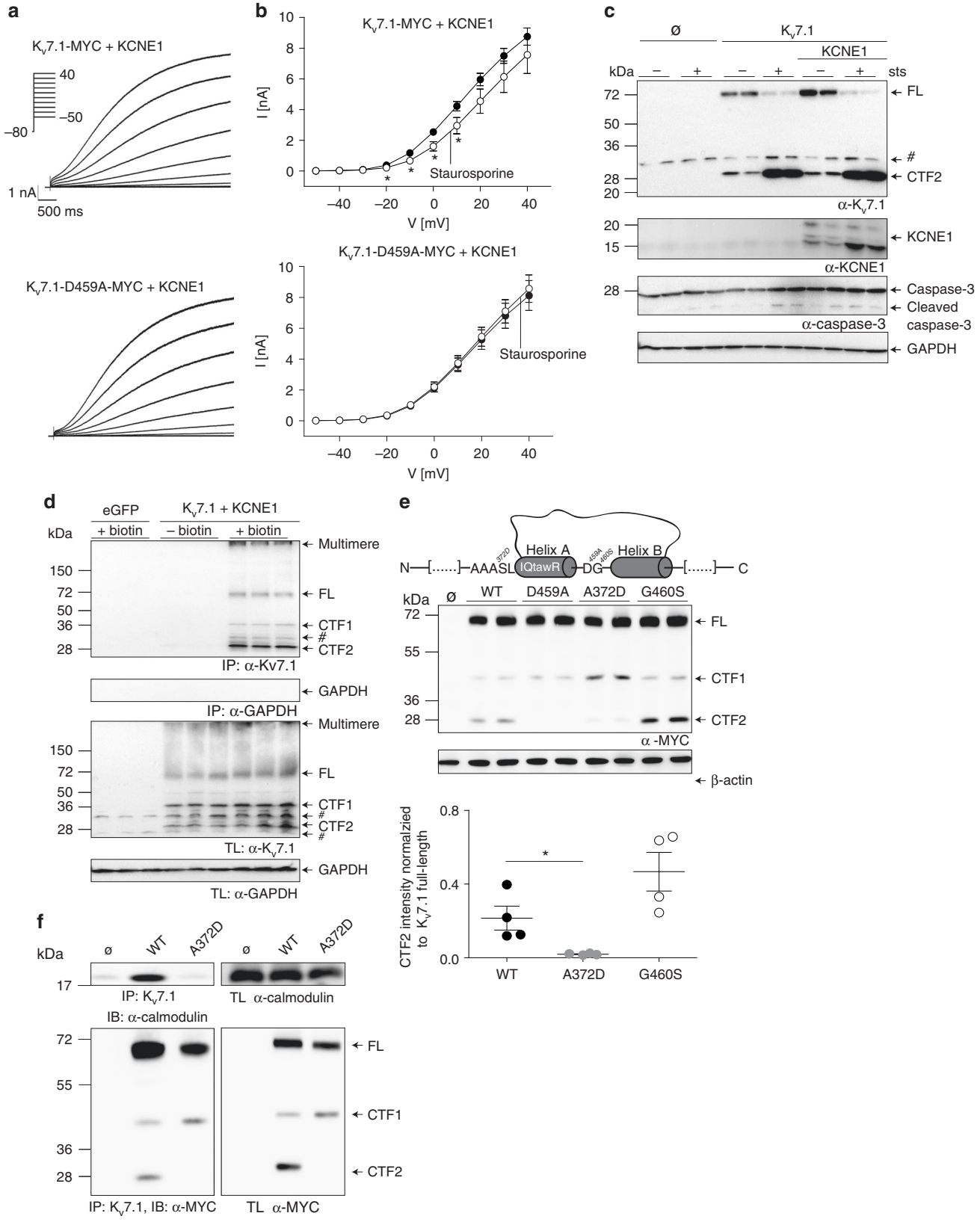

Discussion

To date, over 1500 caspase cleavage sites and substrates have been identified[41]. The vast majority of caspase-mediated cleavage occurs during apoptosis, but caspase function has also been demonstrated in nonapoptotic cellular responses[42], suggesting that caspases cleave a specific subset of substrates independent of apoptosis. Here, we report $K_v7.1$ as a novel substrate for caspases, representing to our knowledge the first example of a voltage-gated cation channel undergoing caspase-mediated proteolysis. However, the transient receptor potential melastin-like 7 (TRMP7) has

Fig. 4 Cleavage of $K_v7.1$ in physiology and pathophysiology. **a** Representative current traces for $K_v7.1$-MYC and $K_v7.1$-D459A-MYC, both coexpressed with KCNE1. **b** Mean currents amplitude was plotted versus voltage to obtain current−voltage (I−V) relationships in cells expressing $K_v7.1$-MYC ($n = 39$ for vehicle, $n = 16$ for staurosporine treatment) or $K_v7.1$-D459A-MYC ($n = 27$ for vehicle, $n = 17$ for staurosporine treatment) and KCNE1 treated with 500 nmol per L staurosporine for 10–12 h. Statistics were tested with two-way ANOVA followed by Bonferroni post-tests. **c** Immunoblot analysis of HeLa cells coexpressing Kv7.1 with KCNE1-MYC treated with 1 µM staurosporine for 4.5 h. Untransfected (Ø) and vehicle-treated cells served as negative controls. **d** Biotinylating study analyzed by immunoblots of Hek 293 cells coexpressing $K_v7.1$ and KCNE1-MYC treated with 1 µM staurosporine for 3 h. Untransfected (Ø) cells as well as cells not treated with biotin served as negative controls. IP Immunoprecipitation. TL total lysate. **e** Schematic illustration to highlight the position of G460 and A372 and calmodulin binding site in helix A. Western blot analysis of HeLa cell lysates overexpressing indicated constructs. Untransfected (Ø) and $K_v7.1$-D459A-transfected cells served as negative controls. Densitometric analysis of four independent experiments of CTF2 band intensity normalized to $K_v7.1$ full-length band intensity. Statistics were tested with one-way-ANOVA followed by Bonferroni's Multiple Comparison test. **f** Coimmunoprecipitation study analyzed by immunoblots of HeLa cells overexpressing wild-type $K_v7.1$ and the A372D mutant with endogenous calmodulin. IP Immunoprecipitation with anti-$K_v7.1$ antibody, IB Immunoblot, TL total lysate. Untransfected cells (Ø) served as negative control. **c** Anti-KCNE1 antibody, anti-caspase 3 antibody. **c**, **d** Anti-$K_v7.1$ antibody, anti-GAPDH antibody. **e** Anti-β-actin antibody. **e**, **f** Anti-MYC antibody. **f** Anti-calmodulin antibody. All graphs are shown as mean and error bars as SEM

been also identified as a caspase substrate, which appears to be critical for Fas-induced apoptosis[43].

Cleavage of human $K_v7.1$ by caspases occurs after an aspartate at position 459, which is located within the intervening loop between helices A and B in the channel's large cytoplasmic C-terminal domain that serves as a scaffold for numerous protein −protein interactions involved in cellular signaling cascades[15]. Both helices appear to form a two-helical bundle, which is embraced by a calmodulin molecule as revealed by X-ray crystallography of recombinantly expressed calmodulin and the proximal C-terminus of $K_v7.1$[34]. In this study, the intervening loop, in which the caspase-mediated proteolysis of $K_v7.1$ occurs, was deleted. Thus, structural information about the caspase cleavage site is missing so far. However, our finding that the calmodulin binding-deficient Kv7.1 A372D mutant is not processed by caspases strongly suggest that calmodulin either helps to recruit caspases to the channel complex or determines the structure of the intervening loop necessary for proper caspase recognition.

Our functional analysis using patch-clamp suggests that caspase cleavage interferes with the function of $K_v7.1$. This finding is supported by numerous reports showing that the intracellular C-terminal domain of $K_v7.1$ is responsible for channel tetramerization, trafficking and modulating the biophysical properties of the channel[15]. The rather small effect of Kv7.1 cleavage on whole-cell currents could be explained by the continued association of CTF2 with the apoprotein complex. For example, calmodulin could, by binding to helices A and B, act as a bridging molecule. Alternatively, the interaction of CTF2 via helices C and D with uncleaved Kv7.1 subunits could keep CTF2 in the channel complex. However, our cell surface biotinylation data strongly suggest that CTF2 is still present in heteromeric Kv7.1/KCNE1 localized at the plasmalemma.

Many pathogenic LQT1 mutations have been mapped to the C-terminus of $K_v7.1$ emphasizing the functional importance of this particular channel region[44]. Our finding that the LQT1 mutation G460S, which is adjacent to the aspartate 459 residue, is more susceptible to caspase cleavage suggest a potential novel pathophysiologic mechanism for LQT1 mutations located in the C-terminus of $K_v7.1$.

Based on the analysis of a number of cleavage sites, a general consensus motif of DXED-A/G/S/T has been proposed for apoptosis executioner caspases such as caspases 3 and 7, whereas caspases 2, 8, 9, and 10 and caspases 1, 4, 5, 6, and 14, prefer isoleucine/ leucine or tryptophan/tyrosine/valine instead of an aspartate at the first position, respectively[41]. Due to the overlapping specificity of caspases and the significantly different $K_v7.1$ cleavage site (amino acid sequence: FSVD-G), it is difficult to predict which individual caspase cleaves $K_v7.1$. Our coexpression data suggest that $K_v7.1$ can be cleaved by all tested caspases including caspases 1, 2, 3, 7 and 8. In this group, caspase 1 was more efficient in $K_v7.1$ processing, which is in agreement with the larger similarity of the preferred cleavage site[41].

Caspases have well-established functions in the execution of apoptosis, as well as inflammation[28]. However, transiently active caspases have also been detected in nonapoptotic cells. For example, in neurons, caspases 3 and 9 are critical for long-term depression and AMPA receptor internalization[32]. In the heart, increased expression of caspase 1 was found in murine heart failure models and in patients with end-stage heart failure[31]. Analysis of mice with heart-targeted overexpression of caspases 1 and 3 further supported the notion that caspases contribute to heart diseases, likely based on an overlap of apoptotic and non-apoptotic functions[30,31]. Our finding that I_{Ks} is sensitive to caspase-mediated cleavage uncovers a novel molecular mechanism that may contribute to cardiac arrhythmias, which is strongly supported by an increased susceptibility of the LQT1 G460S mutant to proteolytic processing by caspases. Thus, it is likely that the reported 40% smaller current density of the G460S mutant, when compared to wild-type I_{Ks}, is at least partially due to an increased cleavage of the mutant[39]. Although several C-terminally located LQT1 mutations have been identified which interfere with channel function by modulating calmodulin[16,45] or phosphatidylinositol 4,5-bisphosphate[46] binding and/or disrupt assembly of functional I_{Ks}[15], for most of the C-terminal LQT mutations, the pathophysiological mechanism that leads to disease is unknown. Our data strongly suggest that susceptibility to caspase-mediated degradation should also be considered when analyzing these mutations.

Furthermore, our results demonstrate that doxorubicin treatment of human-induced pluripotent stem cell-derived cardiomyocytes efficiently induced caspase-mediated cleavage of $K_v7.1$, suggesting that this pathway might contribute to doxorubicin-induced cardiotoxicity. Interestingly, doxorubicin has also been shown to induce electrocardiogram abnormalities such as QT interval prolongations, which are often observed within the first day after chemotherapy[25]. These results have been confirmed in animal studies, showing that doxorubicin prolongs the cardiac action potential duration by specifically inactivating I_{Ks} but not I_{Kr}, which both compose the delayed rectifier potassium current I_K[23]. In cardiomyocytes, I_{Ks} is mediated by a macromolecular complex formed by assembly of the pore-forming subunits $K_v7.1$ with KCNE1 β-subunits, which are linked to the scaffolding protein yotiao/A-kinase anchoring protein 9 (AKAP-9)[20]. Yotiao binds to the distal part of the C-terminus of $K_v7.1$ and recruits PKA, protein phosphatase 1 (PP1), adenylate cyclase 9 (AC9) and phosphodiesterase PDE4D3 to the complex, allowing the control of the phosphorylation state of $K_v7.1$, which is the molecular basis

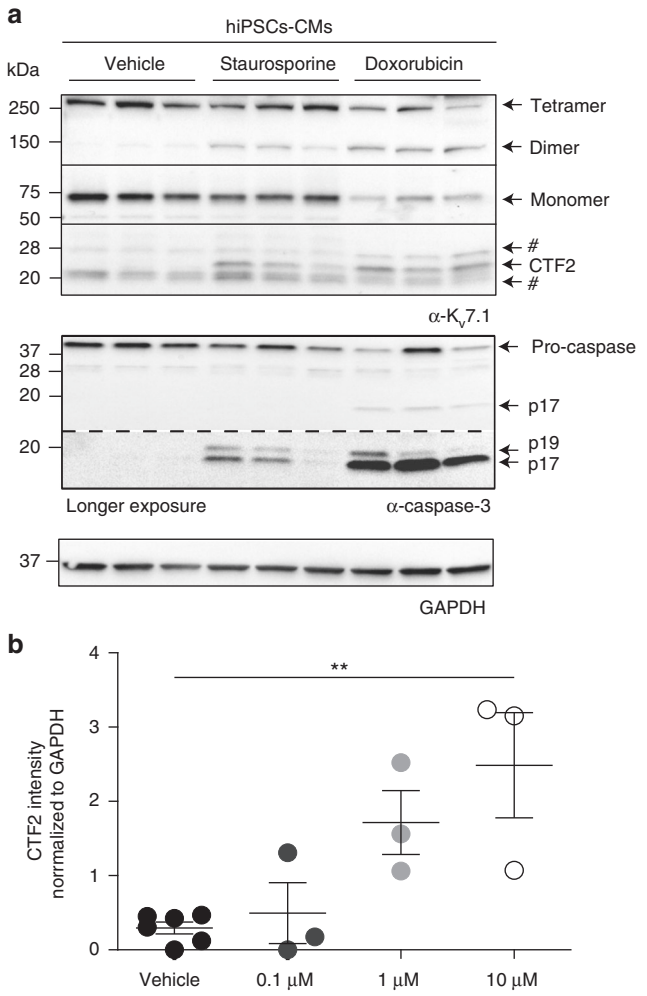

Fig. 5 Doxorubicin induces cleavage of Kv7.1 to CTF2. **a** Immunoblot analysis of human-induced pluripotent stem cell-derived cardiomyocytes treated either with vehicle, staurosporine (2 μM) for 4 h or doxorubicin (10 μM) overnight. # indicates nonspecific binding of the K_v7.1 antibody. **b** Densitometric analysis of 3–6 independent experiments of band intensities of CTF2 normalized to GAPDH band intensity. Statistics were tested with one-way-ANOVA followed by Bonferroni's Multiple Comparison test. **a** Anti-K_v7.1 antibody, anti-caspase-3 antibody, anti-GAPDH antibody. All dot blots are shown as mean and error bars as SEM

for the β-adrenergic regulation of I_{Ks}[20,47]. In silico sequence analyses of yotiao predict several potential caspase cleavage sites, suggesting that this scaffold protein is also processed by caspases[41]. Thus, it is conceivable that caspase-mediated processing of K_v7.1 and likely yotiao contributes to the prolongation of the QT interval mediated by doxorubicin. It will be important to determine the pathway by which doxorubicin treatment leads to elevated caspase activity and K_v7.1 cleavage. While it is widely accepted that doxorubicin-induced cardiotoxicity is due to the induction of mitochondrial dysfunction, resulting in an increased production of ROS in the cytoplasm and consequent activation of extrinsic and intrinsic apoptotic pathways, a more direct effect on ROS-mediated signaling by the oxidizing activity of doxorubicin on Fe^{2+} ions, as suggested by the alleviating effect of dexrazoxane, must also be considered. This will also clarify the issue of whether regulated C-terminal cleavage of K_v7.1 is more generally involved in ROS-mediated cardiac responses.

In summary, the present study demonstrates caspase-mediated proteolysis of K_v7.1. Posttranslational modifications such as phosphorylation, ubiquitination, sumoylation, palmitoylation, and glycosylation have been reported for potassium channels[48]. According to our data, proteolysis of K_v7.1 mediated by caspases is another important mechanism of posttranslational modification of K_v7.1, and we hypothesize that analysis of this regulation will advance understanding of the molecular mechanism of doxorubicin-induced cardiotoxicity.

Methods

Plasmids and antibodies. Human K_v7.1 and caspase cDNAs were subcloned in the expression vectors pFrog and pcDNA4/TO (Invitrogen, Waltham, USA), respectively. Mutations, deletions and tags for antibodies were constructed/introduced by recombinant PCR and verified by sequencing. The C-terminal anti-K_v7.1 antibody was directed against the following peptide sequence TVPRRGPDEGS. The following antibodies were used: rabbit anti-β-actin (A2066, Sigma-Aldrich, St. Louis, USA), rabbit anti-caspase 3 (8G10, Cell Signaling, Cambridge, UK), rabbit anti-calmodulin (ab45689, Abcam, Cambridge, UK), rabbit anti-Eef2 (eukaryotic translation elongation factor 2, ab33523, Abcam, Cambridge, UK), mouse anti-GAPDH (MAB374, Millipore, Billerica, USA), rabbit anti-KCNE1 (APC-163, Alomone Labs, Jerusalem, Israel), rabbit anti-K_v7.1 (ab77701, Abcam, Cambridge, UK), mouse anti-MYC (9B11, Cell Signaling, Cambridge, UK), goat anti-MYC (GTX29106, GeneTex Inc., Irvine, USA).

Cell culture, transfection, and inhibitors. HEK 293T, HeLa, Cos7, and MCF-7 (ATCC, Manassas, USA) were grown in Dulbecco's modified Eagle's medium (DMEM, Thermo Fisher Scientific) supplemented with 10% fetal bovine serum (FBS, Biochrome, Berlin, Germany), 100 U per mL penicillin and 100 μg per mL streptomycin (both Carl Roth, Karlsruhe, Germany). For HL-1 cells (gift from W.C. Claycomb), Claycomb medium (Sigma-Aldrich), supplemented with 10% FBS (Biochrome), 100 U per mL penicillin, 100 μg per mL streptomycin, 0.1 mM norepinephrine (Carl Roth) and 2 mM L-Glutamine (Carl Roth) was used. All cells were kept at 37 °C and 5% CO_2. Transient transfections were performed using TurboFect (Thermo Fischer Scientific) according to the manufacturer's instructions, and stable cell lines were established using G418 for selection. Inhibitors were used as follows: Z-VAD-FMK (12 h, 100 μM, Promega, Fitchberg, USA), Q-VD-OPh (12 h, 450 nM, Merck Millipore, Billerica, USA), staurosporine (1 to 8 h, 0.5–2 μM, Sigma-Aldrich), caspase-8 inhibitor II (2 h pretreatment, 20 or 50 μM, Calbiochem, Billerica, USA), Doxorubicin (overnight, 0.1 μM–10 μM, Sigma-Aldrich).

Protein extraction, immunoprecipitation, and immunoblotting. Cells were washed twice with phosphate-buffered saline (PBS) and harvested in PBS, containing a protease inhibitor cocktail (Complete, Roche, Basel, Switzerland). After centrifugation, cell pellets were lysed in PBS/Complete (1% Triton X-100, Carl Roth) by sonication. After 1 h incubation on ice, samples were centrifuged, and supernatants were analyzed by SDS-PAGE. For coimmunoprecipitations and immunoprecipitations, cells were lysed in EBC buffer/Complete (120 mM NaCl, 50 mM Tris-HCl, 0.5% NP-40, pH 7.4 (all from Carl Roth)) and treated as described above. Lysates were incubated with mouse anti-MYC antibody (coimmunoprecipitation) or treated with K_v7.1-myc antibody (immunoprecipitation) at 4 °C overnight. For precipitation, protein G agarose beads (coimmunoprecipitation) or protein G dynabeads (immunoprecipitation) were used. After thorough washing of the beads, protein complexes were released by denaturation. Samples were subjected to SDS-PAGE and transferred onto nitrocellulose membranes by tank blotting. Membranes were blocked and incubated overnight at 4 °C in primary antibody solution followed by incubation with the appropriate secondary antibodies conjugated to horseradish peroxidase. After thorough washing, bound antibodies were detected by chemiluminescence using a luminescent imager (LAS-4000, Fujifilm, GE Healthcare, Little Chalfont, UK). For quantifications, ImageJ software was used.

Biotinylating assay. After washing cells twice with PBS/CM (0.1 mM $CaCl_2$, 1 mM $MgCl_2$), cells were incubated with 0.5 mg NHS biotin ester (Thermo Fisher) in PBS/CM for 10 min. By adding 50 mM Glycin in PBS/CM biotinylation was stopped. After two washing steps with PBS/CM, cells were lysed as described for immunoprecipitation studies above. Incubation with Streptavidin beads for 1 h at 4 °C was used to precipitate biotinylated proteins. After through washing proteins were released by denaturation and subjected to SDS-PAGE and immunoblotting as described above.

Isolation of neonatal rat ventricular cardiomyocytes. Hearts of 1–2-day-old Wistar rats were harvested and minced in buffer (120 mmol NaCl, 20 mmol HEPES, 8 mmol NaH_2PO_4, 6 mmol glucose, 5 mmol KCl, 0.8 mmol $MgSO_4$, pH = 7.4). Subsequently, up to six digestion steps were carried out with 0.6 mg per mL pancreatin (Sigma-Aldrich) and 0.5 mg per mL collagenase type II (Worthington, Lakewood, USA) in sterile ADS buffer. Cardiomyocytes were purified from contaminating fibroblasts using a Percoll gradient centrifugation step. Finally,

NRVMs were resuspended and cultured in DMEM containing 10% FBS, 100 U per mL penicillin, 100 µg per mL streptomycin and 1% L-Glutamine. Protein extractions were performed as described above.

Human-induced pluripotent stem cell culture. Human-induced pluripotent stem cell-derived cardiomyocytes[49] were routinely maintained in E8 medium implemented with 10 µM Rho kinase inhibitor (Y27632; Biorbyt, Cambridge, UK) for the first 24 h after passage on 1:400 reduced growth factor Matrigel (Corning, Corning, USA). Cells were passaged ~1:15 every 3–4 days using 0.5 mM EDTA in Dulbecco's PBS (DPBS; Corning, Corning, USA) after achieving ~80% confluence. Cell lines were used between passages 20 and 85. All cultures were routinely tested for mycoplasma using a MycoAlert PLUS Kit (Lonza, Basel, Switzerland).

Cardiac differentiation from human iPS cells. Cardiac differentiation was performed as described previously[49]. Briefly, to initiate differentiation, medium was changed to CDM3, consisting of RPMI 1640 (Corning), 500 µg ml^{-1} *Oryza sativa*-derived recombinant human albumin (Oryzogen, Wuhan, China), and 213 µg ml^{-1} L–ascorbic acid 2-phosphate (Wako, Tokyo, Japan). For days 0–1, media was supplemented with 3 µM of the glycogen synthase kinase 3β inhibitor CHIR99021 (Biorbyt, San Francisco, USA)[21,22] and 10 ng ml^{-1} BMP4 (Peprotech, Hamburg, Germany). On day 1, media was changed to CDM3 and on d2 media was changed to CDM3 supplemented with 2 µM of the Wnt inhibitor Wnt-C59 (Biorbyt). Media was changed on day 4 and every other day thereafter with CDM3. Contracting cells were noted from day 7. At days 25–29, contracting cardiomyocytes were dissociated by incubating 20 min in DPBS followed by 6 min in TrypLE (Thermo Fisher Scientific), and then 60 min with 0.5 U per mL Liberase TH (Roche) in CDM3 media. Cells were replated in 40% FBS in CDM3 by combining 2–3 wells into one well for optimal viability of the cultures. After 2 days, media was changed back to CDM3 and exchanged every 2 days until analysis.

Electrophysiology. Transfected cells were identified by using cotransfection of eGFP and imaging on an inverted fluorescence microscope (Axiovert 40, Zeiss, Jena, Germany) with a fiber optic-coupled light source (UVICO, Rapp OptoElectronic, Hamburg, Germany). Current signals were recorded in whole-cell patch-clamp mode at room temperature (22 ± 1 °C) 2 days after transfection. Recordings were started 3 min after whole-cell access was obtained. Data were sampled at 20 kHz and filtered at 5 kHz, using an Axopatch 200B amplifier in combination with a Digidata 1322A interface and pClamp10 software (all from Molecular Devices/MDS Analytical Technologies, Sunnyvale, USA). Electrodes were made from borosilicate glass (Harvard Apparatus, Edenbridge, UK or BioMedical Instruments, Zoellnitz, Germany), using a DMZ-Universal Puller (Zeitz, Munich, Germany). Pipette resistance in bath solution was 2.0–3.5 MΩ and access resistance was typically <5 MΩ before series resistance compensation (75%). External solution contained (in mM): 145 NaCl, 4 KCl, 2 $CaCl_2$, 2 $MgCl_2$, 10 D-glucose, 10 HEPES, adjusted to pH 7.4 with NaOH. The internal solution was composed of (in mM) 135 K-gluconate, 4 NaCl, 10 KCl, 5 Hepes, 5 EGTA, 2 Na_2-ATP, 0.3 Na_3-GTP (pH 7.25 with KOH). Cells were incubated with staurosporine at a concentration of 500 nM 10–12 h before recordings. Chemicals were purchased from Sigma-Aldrich.

Statistics. Data are shown as means ± SEM of n observations, as indicated. Statistical analyses were performed using unpaired two-tailed Student's t test, one-way ANOVA and Bonferroni's Multiple Comparison post hoc test or two-way ANOVA followed by Bonferroni post-tests, where applicable, using the GraphPad Prism 5 software (GraphPad, San Diego, USA). $p \le 0.05$ was termed significant. $^{*}0.01 \le p \le 0.05$. $^{**}0.001 \le p < 0.01$. $^{***}p < 0.001$.

Data availability

The authors declare that the data supporting the findings of this study are available within the paper and its supplementary information files.

Received: 6 March 2018 Accepted: 31 August 2018
Published online: 28 September 2018

References

1. Yu, F. H., Yarov-Yarovoy, V., Gutman, G. A. & Catterall, W. A. Overview of molecular relationships in the voltage-gated ion channel superfamily. *Pharmacol. Rev.* **57**, 387–395 (2005).
2. Jentsch, T. J., Schroeder, B. C., Kubisch, C., Friedrich, T. & Stein, V. Pathophysiology of KCNQ channels: neonatal epilepsy and progressive deafness. *Epilepsia* **41**, 1068–1069 (2000).
3. Lehman, A. et al. Loss-of-function and gain-of-function mutations in KCNQ5 cause intellectual disability or epileptic encephalopathy. *Am. J. Hum. Genet.* **101**, 65–74 (2017).
4. Wang, Q. et al. Positional cloning of a novel potassium channel gene: KVLQT1 mutations cause cardiac arrhythmias. *Nat. Genet.* **12**, 17–23 (1996).
5. Neyroud, N. et al. A novel mutation in the potassium channel gene KVLQT1 causes the Jervell and Lange-Nielsen cardioauditory syndrome. *Nat. Genet.* **15**, 186–189 (1997).
6. Chen, Y. H. et al. KCNQ1 gain-of-function mutation in familial atrial fibrillation. *Science* **299**, 251–254 (2003).
7. Barhanin, J. et al. K(V)LQT1 and lsK (minK) proteins associate to form the I (Ks) cardiac potassium current. *Nature* **384**, 78–80 (1996).
8. Sanguinetti, M. C. et al. Coassembly of K(V)LQT1 and minK (IsK) proteins to form cardiac I(Ks) potassium channel. *Nature* **384**, 80–83 (1996).
9. Unoki, H. et al. SNPs in KCNQ1 are associated with susceptibility to type 2 diabetes in East Asian and European populations. *Nat. Genet.* **40**, 1098–1102 (2008).
10. Yasuda, K. et al. Variants in KCNQ1 are associated with susceptibility to type 2 diabetes mellitus. *Nat. Genet.* **40**, 1092–1097 (2008).
11. Roepke, T. K. et al. Kcne2 deletion uncovers its crucial role in thyroid hormone biosynthesis. *Nat. Med.* **15**, 1186–U1117 (2009).
12. Schroeder, B. C. et al. A constitutively open potassium channel formed by KCNQ1 and KCNE3. *Nature* **403**, 196–199 (2000).
13. Than, B. L. et al. The role of KCNQ1 in mouse and human gastrointestinal cancers. *Oncogene* **33**, 3861–3868 (2014).
14. den Uil, S. H. et al. Loss of KCNQ1 expression in stage II and stage III colon cancer is a strong prognostic factor for disease recurrence. *Br. J. Cancer* **115**, 1565–1574 (2016).
15. Haitin, Y. & Attali, B. The C-terminus of Kv7 channels: a multifunctional module. *J. Physiol.* **586**, 1803–1810 (2008).
16. Shamgar, L. et al. Calmodulin is essential for cardiac IKS channel gating and assembly: impaired function in long-QT mutations. *Circ. Res.* **98**, 1055–1063 (2006).
17. Schwake, M., Jentsch, T. J. & Friedrich, T. A carboxy-terminal domain determines the subunit specificity of KCNQ K+ channel assembly. *EMBO Rep.* **4**, 76–81 (2003).
18. Schmitt, N. et al. A recessive C-terminal Jervell and Lange-Nielsen mutation of the KCNQ1 channel impairs subunit assembly. *EMBO J.* **19**, 332–340 (2000).
19. Schwake, M. et al. Structural determinants of M-type KCNQ (Kv7) K+channel assembly. *J. Neurosci.* **26**, 3757–3766 (2006).
20. Marx, S. O. et al. Requirement of a macromolecular signaling complex for beta adrenergic receptor modulation of the KCNQ1-KCNE1 potassium channel. *Science* **295**, 496–499 (2002).
21. Jespersen, T. et al. The KCNQ1 potassium channel is down-regulated by ubiquitylating enzymes of the Nedd4/Nedd4-like family. *Cardiovasc. Res.* **74**, 64–74 (2007).
22. Xiong, D. et al. SUMOylation determines the voltage required to activate cardiac IKs channels. *Proc. Natl. Acad. Sci. USA* **114**, E6686–E6694 (2017).
23. Ducroq, J. et al. Dexrazoxane protects the heart from acute doxorubicin-induced QT prolongation: a key role for I(Ks). *Br. J. Pharmacol.* **159**, 93–101 (2010).
24. Octavia, Y. et al. Doxorubicin-induced cardiomyopathy: from molecular mechanisms to therapeutic strategies. *J. Mol. Cell. Cardiol.* **52**, 1213–1225 (2012).
25. Renu, K., V, G. A., P, B. T. & Arunachalam, S. Molecular mechanism of doxorubicin-induced cardiomyopathy—an update. *Eur. J. Pharmacol.* **818**, 241–253 (2017).
26. Hasinoff, B. B., Schroeder, P. E. & Patel, D. The metabolites of the cardioprotective drug dexrazoxane do not protect myocytes from doxorubicin-induced cytotoxicity. *Mol. Pharmacol.* **64**, 670–678 (2003).
27. Poreba, M., Strozyk, A., Salvesen, G. S. & Drag, M. Caspase substrates and inhibitors. *Cold Spring Harb. Perspect. Biol.* **5**, a008680 (2013).
28. McIlwain, D. R., Berger, T. & Mak, T. W. Caspase functions in cell death and disease. *Cold Spring Harb. Perspect. Biol.* **5**, a008656 (2013).
29. Zhang, J. H., Zhang, Y. & Herman, B. Caspases, apoptosis and aging. *Ageing Res. Rev.* **2**, 357–366 (2003).
30. Condorelli, G. et al. Heart-targeted overexpression of caspase3 in mice increases infarct size and depresses cardiac function. *Proc. Natl. Acad. Sci. USA* **98**, 9977–9982 (2001).
31. Merkle, S. et al. A role for caspase-1 in heart failure. *Circ. Res.* **100**, 645–653 (2007).
32. Li, Z. et al. Caspase-3 activation via mitochondria is required for long-term depression and AMPA receptor internalization. *Cell* **141**, 859–871 (2010).
33. Aram, L. et al. A Krebs cycle component limits caspase activation rate through mitochondrial surface restriction of CRL activation. *Dev. Cell* **37**, 15–33 (2016).
34. Sachyani, D. et al. Structural basis of a Kv7.1 potassium channel gating module: studies of the intracellular c-terminal domain in complex with calmodulin. *Structure* **22**, 1582–1594 (2014).
35. Tommiska, J. et al. Two missense mutations in KCNQ1 cause pituitary hormone deficiency and maternally inherited gingival fibromatosis. *Nat. Commun.* **8**, 1289 (2017).

36. Rawlings, N. D., Barrett, A. J. & Finn, R. Twenty years of the MEROPS database of proteolytic enzymes, their substrates and inhibitors. *Nucleic Acids Res.* **44**, D343–D350 (2016).
37. Janicke, R. U., Sprengart, M. L., Wati, M. R. & Porter, A. G. Caspase-3 is required for DNA fragmentation and morphological changes associated with apoptosis. *J. Biol. Chem.* **273**, 9357–9360 (1998).
38. Claycomb, W. C. et al. HL-1 cells: a cardiac muscle cell line that contracts and retains phenotypic characteristics of the adult cardiomyocyte. *Proc. Natl. Acad. Sci. USA* **95**, 2979–2984 (1998).
39. Arnestad, M. et al. Prevalence of long-QT syndrome gene variants in sudden infant death syndrome. *Circulation* **115**, 361–367 (2007).
40. Ueno, M. et al. Doxorubicin induces apoptosis by activation of caspase-3 in cultured cardiomyocytes in vitro and rat cardiac ventricles in vivo. *J. Pharmacol. Sci.* **101**, 151–158 (2006).
41. Kumar, S., van Raam, B. J., Salvesen, G. S. & Cieplak, P. Caspase cleavage sites in the human proteome: CaspDB, a database of predicted substrates. *PLoS ONE* **9**, e110539 (2014).
42. Kuranaga, E. Beyond apoptosis: caspase regulatory mechanisms and functions in vivo. *Genes Cells* **17**, 83–97 (2012).
43. Desai, B. N. et al. Cleavage of TRPM7 releases the kinase domain from the ion channel and regulates its participation in Fas-induced apoptosis. *Dev. Cell* **22**, 1149–1162 (2012).
44. Moss, A. J. & Kass, R. S. Long QT syndrome: from channels to cardiac arrhythmias. *J. Clin. Invest.* **115**, 2018–2024 (2005).
45. Ghosh, S., Nunziato, D. A. & Pitt, G. S. KCNQ1 assembly and function is blocked by long-QT syndrome mutations that disrupt interaction with calmodulin. *Circ. Res.* **98**, 1048–1054 (2006).
46. Park, K. H. et al. Impaired KCNQ1-KCNE1 and phosphatidylinositol-4,5-bisphosphate interaction underlies the long QT syndrome. *Circ. Res.* **96**, 730–739 (2005).
47. Chen, L., Kurokawa, J. & Kass, R. S. Phosphorylation of the A-kinase-anchoring protein Yotiao contributes to protein kinase A regulation of a heart potassium channel. *J. Biol. Chem.* **280**, 31347–31352 (2005).
48. Huang, X. & Jan, L. Y. Targeting potassium channels in cancer. *J. Cell. Biol.* **206**, 151–162 (2014).
49. Burridge, P. W. et al. Chemically defined generation of human cardiomyocytes. *Nat. Methods* **11**, 855–860 (2014).

Acknowledgements

We thank Maike Langer, Vanessa Mangels, and Marvin Murowski for excellent technical assistance; William C. Claycomb for the HL-1 cells and Jakob Völkl, Florian Lang, and Karl E. Pfeifer for $K_v7.1$-deficient murine tissues. This work was supported by the Deutsche Forschungsgemeinschaft (Grant SFB 877, B8 and Heisenberg Fellowship to M.S.). We acknowledge support for the Article Processing Charge by the Deutsche Forschungsgemeinschaft and the Open Access Publication Fund of Bielefeld University.

Author contributions

A.S., C.R., and M.S. designed the study. A.S., C.R., S.H., T.H., A.J.T.S. performed experiments and data analysis. T.H., A.J.T.S., C.A., T.F., P.W.B., M.L., and M.S. interpreted the data and edited the manuscript. A.S., C.R., T.F., and M.S. wrote the manuscript with contributions from all authors.

Additional information

Supplementary information accompanies this paper at https://doi.org/10.1038/s42003-018-0162-z.

Competing interests: The authors declare no competing interests.

Reprints and permission information is available online at http://npg.nature.com/reprintsandpermissions/

Publisher's note: Springer Nature remains neutral with regard to jurisdictional claims in published maps and institutional affiliations.